Accepted Manuscript

http://dx.doi.org/10.1006/jssc.1999.8336

J. Schmedt auf der Günne, S. Kaczmarek, L. van Wüllen, H. Eckert, D. Paschke, A. J. Foecker, and W. Jeitschko. Solid state NMR connectivity studies in dipolarly coupled inorganic networks: Crystal structure and site assignments for the lithium phosphide LiP_5. *J. Solid State Chem.*, 147:341--349, 1999.

Solid State NMR Connectivity Studies in Dipolarly Coupled Inorganic Networks: Crystal Structure and Site Assignments for the Lithium Polyphosphide LiP_5

Jörn Schmedt auf der Günne, Sylvia Kaczmarek, Leo van Wüllen, and Hellmut Eckert*

Institut für Physikalische Chemie
Westfälische Wilhelms-Universität Münster
Schlossplatz 7
D-48149 Münster, Germany

Dirk Paschke, Aloys J. Foecker, and Wolfgang Jeitschko*

Institut für Anorganische Chemie
Westfälische Wilhelms-Universität Münster
Wilhelm-Klemm-Strasse 8
D-48149 Münster, Germany

Dedicated to the memory of JEAN ROUXEL

Abstract

The crystal structure of LiP_5 has been refined from single-crystal X-ray data to a residual of $R = 0.020$ for 2357 structure factors and 56 variable parameters. The structure as determined in the acentric space group $Pna2_1$ by v. Schnering and Wichelhaus (1972) is confirmed. However, the lithium position has been determined with considerably greater accuracy. The polyanionic network of the phosphorus atoms can also be refined in the corresponding centrosymmetric group *Pnam*, where two adjacent lithium positions with partial occupancy are found. The phosphorus connectivities within this network are studied by means of advanced solid state NMR techniques. Crystalline polyphosphides represent a particular challenge for such experiments owing to the presence of strong homonuclear ^{31}P-^{31}P dipole-dipole couplings within the network of phosphorus polyanions. To meet this challenge a powerful strategy has been designed by combining magic-angle spinning with ^{31}P-^{31}P double-quantum-filtered 2-D exchange, rotational resonance, and heteronuclear crosspolarization spectroscopies. Based on this information, the NMR results are discussed in connection with the local environments of the phosphorus sites.

Introduction

The great structural variety of inorganic phosphides has intrigued solid state chemists and crystallographers for many decades (1-3). In recent years, the optical, electrical and opto-electronic properties of phosphides have generated considerable attention, making these compounds potentially interesting materials for applications in information technologies (4-7). The crystalline solid state is frequently characterized by various types of stacking defects, order/disorder phenomena, and deviations from perfect stoichiometries. In addition, some phosphide systems are known to form extended solid solutions and/or glasses (8). To date, structural issues in these materials have been studied primarily by diffraction techniques.

During the past two decades magic-angle-spinning (MAS) solid state NMR has emerged as a powerful spectroscopic technique for structural studies of many disordered materials (9). Also inorganic crystalline phosphides have been subject of many investigations (10-21). However, while MAS-NMR is able to discern, characterize, and quantify distinct local environments present in a wide range of solids, it cannot provide any information about connectivities or spatial proximity among distinct sites. Most recently, the development of advanced multi-dimensional and/or double resonance techniques has allowed such questions to be addressed. These methods combine the advantages of MAS-NMR with the measurement of dipole-dipole interactions, which are sensitive to internuclear distances. However, applications of such techniques to phosphides have to date been scarce and limited in scope (22-25), which seems surprising in view of the favorable NMR characteristics of the ^{31}P isotope. A serious complication encountered in phosphides is limited resolution due to strong homonuclear ^{31}P-^{31}P dipole-dipole interactions, which are not averaged out completely by even fast

MAS. Additional linebroadening effects arise from unresolved hyperfine structure due to scalar interactions. Part of the objective of the present study is to develop an experimental NMR strategy suitable for addressing structural issues in solids with such strong residual broadening effects.

As a representative model compound we have chosen lithium polyphosphide, LiP_5. The published crystal structure consists of a three-dimensional network constructed by P-P bonds among five crystallographically inequivalent phosphorus sites (26). Here we present a refinement of this structure resulting in more accurate data than previously reported. Using this detailed crystallographic information, we will discuss the NMR results in connection with the local environments of the phosphorus sites.

Sample Preparation and Characterization

Single-phase LiP_5 was prepared by reaction of the elemental components in a closed steel tube (2.4 cm^3), which in turn was sealed in an evacuated silica tube to prevent the reaction with air. A stoichiometric mixture (0.6 g) of lithium pieces (Merck, > 99%) and small pieces of red phosphorus (Hoechst-Knapsack, "ultrapure") was annealed at 500°C for one week. The reaction product consisted of a well crystallized polycrystalline ingot of black LiP_5 and flakes originating from the inner wall of the steel tube. The flakes were identified by a Guinier powder pattern to consist of Fe, Fe_2P, and FeP. They could completely be removed from the crushed LiP_5 ingot by a magnet, even though Fe_2P and FeP are not ferromagnetic at room temperature (27,28). Energy dispersive X-ray fluorescence analyses in a scanning electron microscope did not show any impurity elements heavier than sodium.

The single-crystal of LiP_5 used for the structure refinement was isolated from a sample, which was prepared by reaction of the elemental components (1 week at

550°C) with the atomic ratio Li:P = 1:10 in a sealed silica tube (0.1 g red phosphorus, tube volume 5 cm^3).

Crystal Structure Refinement

The orthorhombic lattice constants of LiP_5 were determined from the Guinier powder data, recorded with CuKα_1 radiation and α-quartz (a = 491.30 pm, c = 540.46 pm) as an internal standard: a = 1043.7(1) pm, b = 658.92(8), c = 654.90(9) pm, and V = 0.45038(9) nm^3. These values agree very well with those determined previously (26) : a = 1043.9 pm, b = 658.4 pm, and c = 654.5 pm; and also with those determined on the four-circle diffractometer: a = 1042.7(1) pm, b = 658.44(5) pm, and c = 654.86(8) pm.

The intensity data for the structure determination of LiP_5 were collected on a four-circle diffractometer with θ/2θ scans, graphite-monochromated MoKα radiation, and a scintillation counter with pulse-height discrimination.

The structure was refined with the program package SHELX-97 (29) using atomic scattering factors, corrected for anomalous dispersion. The weighting scheme accounted for the counting statistics and a parameter correcting for secondary extinction was optimized as a least-squares parameter. The crystallographic data and some results are summarized in Table 1.

The structure as determined in the acentric space group $Pna2_1$, by v. Schnering and Wichelhaus turned out to be correct. However, the position of the lithium atom was obtained with higher accuracy. Its location, as defined by the phosphorus positions of both refinements (which are very similar) differs from the previous location by 36 pm.

It is interesting that the positions of the phosphorus atoms can almost equally well be refined in the corresponding centrosymmetric group *Pnam*, a non-standard

setting of the space group *Pnma* (No. 62). A difference Fourier synthesis calculated with the positions of the phosphorus atoms resulted in two positions for the lithium atoms on both sides of the mirror plane. The results of the least-squares refinement in the centrosymmetric group are listed together with those of the refinement in $Pna2_1$, in the Tables 1 and 2. The lower symmetry space group $Pna2_1$ has to be preferred not only because of the lower residual, but mainly because in this space group the lithium positions are ordered. Table 3 summarizes the direct bond lengths and the bond angles within the polyphosphide network.

Discussion of the Structure

The crystal structure of LiP_5 consists of six-membered phosphorus rings in chair conformation. These rings share edges, thus forming infinite strings, which are bridged via additional phosphorus (P5) atoms to form a three-dimensional nework (Figs. 1 and 2). The lithium atoms are situated between two strings of condensed phosphorus rings with two bridging P5 atoms as closest neighbors. In the refinement of the structure in the centrosymmetric group *Pnam* the lithium atoms occupy a split position (Fig. 3). The Li-Li distance between the two half-occupied positions is 155 pm. It can be expected that at higher temperature the lithium atoms are disordered, jumping between the two adjacent positions. This expected order/disorder phase transition is probably above 300 °C, since a differential scanning calorimetry experiment did not reveal any phase transition up to this temperature. Considering the symmetry change from the expected high-temperature modification with the point group *mmm* to the room-temperature modification with the pyroelectric group *mm*2 such a transition may be classified as a ferroelectric transition.

The lithium atoms can be expected to have transferred their valence electron to the phosphorus network. According to the Zintl-Klemm concept one may expect that one phosphorus atom of the formula unit (the P5 atom) obtains six valence electrons and therefore forms two homopolar bonds (like sulfur in its various modifications), while the other phosphorus atoms form three P-P bonds as in the various modifications of elemental phosphorus. This expectation is confirmed by the experimental structure.

All of the phosphorus atoms have more or less tetrahedral environments (Table 3). It is interesting that the P-P bonds in LiP_5 have differing bond lengths. The two P-P bonds of the P5 atoms are relatively short (217.6 and 217.8 pm) compared to the P-P bonds within the condensed P_6 rings (between 222.2 and 223.3 pm). Of the latter phosphorus atoms the P1 and P2 atoms, which occupy the same phosphorus position in the expected high-temperature modification of LiP_5, have very similar atomic environments. The P3 and P4 atoms have also similar P-P bond distances but differ from each other in the range of P-P-P bond angles encountered.

NMR Studies

Experimental Details. ^{31}P and ^{7}Li solid state NMR characterization was carried out on Bruker DSX-500 and CXP-200 spectrometers equipped with high-speed spinning probes. Aside from single-pulse spectroscopy, the following dipolar NMR methods were applied: (i) ^{31}P 2-D exchange/double quantum filtering spectroscopy, (ii) ^{31}P-^{31}P rotational resonance, and (iii) ^{7}Li-^{31}P heteronuclear crosspolarization. Here, we summarize the experimental conditions used, while the fundamentals of these methods are described further below. The 2-D exchange/double quantum filtering experiments were conducted at 202.43 MHz

using the following parameters: spinning frequency 15 kHz, 90° pulse length 2.4 μs, dwell time in the t_1-dimension: 28.4 μs, length of DQ excitation/reconversion period 133.3μs (2 rotor periods). The C7 sandwich (see below) used for DQ-filtering was preceded and followed by a 30ms delay to allow decay of unwanted coherence before the final 90° detection pulse was applied. The 2-D data were acquired and processed using the States method (31). For each t_1 increment, 8 scans were acquired with a relaxation delay of 169 s. ^{31}P-^{31}P rotational resonance experiments were conducted at 81.02 MHz, using 90° pulses of 5.5μs length. The MAS rotation speed was varied systematically within the limits 7.9 kHz < ν_r < 12.0 kHz, to produce rotational resonance conditions between distinct pairs of resonances. For each experiment, 4 scans were acquired with a recycle delay of 900 s. A standard Bruker dual-channel 4 mm probe was used in the $\{^7Li\}^{31}P$ CPMAS experiments which were carried out using a Bruker CXP-200 NMR spectrometer with a 4.68 T magnet, using a spinning speed of 10 kHz. The resonance frequencies for ^7Li and ^{31}P were 77.78 and 81.00 MHz, respectively. The close proximity of these two resonance frequencies poses a special experimental challenge that has been addressed as previously published (32): The Q-value of the probe was intentionally lowered by adding a 22 kΩ resistor parallel to the sample coil, increasing the band width of the probe, which was tuned to a center frequency at 79.4 MHz. The X channel of the spectrometer was used for generating the ^{31}P pulses. The ^7Li pulses were generated by mixing the 200 MHz pulsed output of the ^1H decoupler with the output of an external synthesizer (PTS 310). The low pass filtered difference frequency signal was amplified with a second X-channel tube amplifier (Bruker). The two radio frequency pulses for ^7Li and ^{31}P were combined after the amplification stage and gated into the X-channel of the MAS probe using a high-frequency switch box. With this setup, 90° pulse lengths of 2.5 μs (100 kHz) were achieved for both nuclei. The CPMAS experiments were conducted at

variable contact times. Spin-locking experiments indicate that the ^{7}Li spin-lattice relaxation time in the rotating frame lies in the vicinity of 40 ms.

MAS-NMR Results. Table 4 summarizes the results from the ^{31}P MAS-NMR experiments. Fig. 4 shows the single pulse ^{31}P MAS NMR spectra at two different spinning speeds. In the ^{31}P NMR spectrum four distinct resonances (peaks "a"-"d") are seen in the ratio 1:2:1:1, at 1.8, -11.5, -29.0 and -127.7 ppm, respectively. The spectra suggest that two of the phosphorus sites have local environments too similar to be resolvable. Inspection of Table 3 suggests that these are the sites P1 and P2, which are structurally very similar. Furthermore, the isolated low-frequency resonance at -127.7 ppm may be assigned to P5, the phosphorus atom interacting most strongly with lithium, since this chemical shift occurs within a spectral region typical for negatively polarized phosphorus species.[12-14,18-20] Finally, an analysis of the spinning sideband pattern intensities reveals that one of the phosphorus resonances (peak "c" at ppm) is characterized by a significantly stronger chemical shift anisotropy compared to peaks "a" and "b" (see Figure 4, top, revealing the widest spinning sideband pattern for this particular resonance). Inspection of Table 3 reveals that this resonance might be assignable to P3, which shows a particularly wide range of P-P-P bond angles quite different from the situation with the other phosphorus sites. We emphasize, however, that assignments based on MAS alone are tentative and require independent confirmation. To this end we utilize the ^{31}P-^{31}P and ^{31}P-^{7}Li dipole-dipole interactions, which can be reintroduced into MAS-NMR by specifically designed techniques as outlined below.

High Resolution Dipolar NMR Methodology. In multispin systems dipole-dipole couplings are best discussed on the basis of dipolar second moments M_2, which in powdered samples are related to structure via the van Vleck equation (33):

$$M_2\,(^{31}P\text{-}^{31}P) = \frac{3}{5}\left(\frac{\mu_0}{4\pi}\right)^2 \gamma^4\hbar^2 I(I+1)\sum_{i\neq j} r_{ij}^{-6}$$

$$M_2(^{31}P\text{-}^{7}Li) = \frac{4}{15}\left(\frac{\mu_0}{\mu\pi}\right)^2 \gamma_I^2\gamma_S^2\hbar^2 S(S+1)\sum_{S} r_{IS}^{-6}$$

Here, γ_I, I, γ_S, and S are the gyromagnetic ratios and the spin quantum numbers of the ^{31}P spins and the ^{7}Li spins, respectively, $\mu_o/4\pi$ and $\hbar$ represent the magnetic permeability constant and Planck's constant, while r_{ij} and r_{IS} are the relevant internuclear distances.

In MAS-NMR, homonuclear dipolar interactions of weak to moderate strength ($M_2 \leq 10^7$ s^{-2}) can be probed by numerous experimental approaches (34-44). However, many of these techniques are unsuitable for the detection of the very strong ^{31}P-^{31}P dipolar couplings in the 3-dimensional P-P bonded networks of crystalline polyphosphides. For example, saturation transfer experiments following selective excitation, a highly successful approach in various phosphates and phosphorus chalcogenides (42,43), are unsuccessful in LiP_5, because of the very rapid spin diffusion among the different ^{31}P sites on the time scale of the experiment. Likewise 2-dimensional double quantum spectroscopy (39,40) faces severe limitations. Very short excitation times are necessary, and the double quantum coherences once excited decay rapidly into higher coherences due to multiple spin-spin interactions. In addition, the sampling rate in the indirect dimension is limited by the requirement to increment the excitation period in rotor synchrony.

As shown below, the assignment problem in LiP_5 is solved by combining three separate dipolar MAS experiments: (i) 2-D exchange/double quantum filtering spectroscopy (44), (ii) rotational resonance (34), and (iii) heteronuclear crosspolarization. The first two experiments are sensitive to homonuclear ^{31}P-^{31}P interactions and thereby carry information on direct phosphorus site connectivities. The last experiment probes phosphorus-lithium site proximities by measuring the ^{31}P-^{7}Li heteronuclear dipolar coupling strengths for each phosphorus site.

Results from 2-D exchange/double quantum filtering spectroscopy. Figure 5 shows the pulse sequence used for 2-D exchange/double quantum filtering spectroscopy, along with the coherence pathways selected by suitable phase cycling (44). The first pulse creates single quantum coherence which is frequency labelled during the evolution period t_1. After the evolution is stopped by the second 90° pulse, a "C7" sandwich of seven 4π pulses per two rotor periods is used to generate double quantum coherence. The second seven-pulse sandwich serves to reconvert this double quantum coherence to zero-quantum coherence, and the final 90° pulse creates observable magnetization, which is acquired during the detection period t_2 (37). Double Fourier-Transformation with respect to t_1 and t_2 produces a two-dimensional spectrum in which the peaks are correlated through homonuclear ^{31}P-^{31}P dipole-dipole coupling. While the intensities of the autocorrelated (diagonal) peaks are reduced by double quantum filtering, the "cross-peak" intensities in the 2-D spectrum reflect the strengths of the pairwise dipole-dipole couplings involved.

Figure 6 shows the result. Owing to the large number of P-P connectivities, the most valuable information is actually the absence or comparatively low intensity of 2-D crosspeaks observed between the peak pairs "a-c" and "b-d". To facilitate a comparison with the structural data, Table 4 lists homonuclear dipolar second moments calculated from eq. (1a) for each individual pair of phosphorus

sites. In this calculation all of the relevant internuclear distances within a range of 20 Å have been included, producing excellent convergence of the lattice sums. Consistent with the preliminary arguments presented above, Fig. 5 allows the following peak assignments: peak "a": P4, peak "b": P1 and P2, peak "c": P3, peak "d": P5.

Further independent confirmation would be highly desirable, however, because Fig. 6 shows a sizeable crosspeak "b-d" even though the structure shows no direct P1/P2 - P5 connectivity. Additional experiments (not shown) reveal that this crosspeak looses in intensity relative to the others if the excitation period is shortened from 4 to 2 rotor periods, indicating that the "b-d" dipolar coupling is weaker than for the other cases. Table 4 confirms that the second moments P1-P5 and P2-P5 are indeed rather sizeable due to longer-range dipolar coupling. We can thus conclude that the buildup of "b-d" double quantum coherence arises under the influence of more remote ^{31}P spins.

Results from ^{31}P-^{31}P Rotational Resonance. Another technique sensitive to homonuclear dipolar interactions is rotational resonance spectroscopy. Here the MAS spinning frequency is adjusted to be equal to an integer multiple of the chemical shift difference between the two resonances involved (34). Under this condition, the energy difference between the spins involved is balanced by the sample rotation, resulting in zero-quantum coherences among the nuclei involved if they are dipolarly coupled. Stimulation of these coherences results in peak broadening, the extent of which depends on the magnitude of the dipolar coupling constant and hence on the internuclear distance.

In the present study, a rotational resonance mapping experiment was carried out, in order to explore the strength of ^{31}P-^{31}P dipole-dipole coupling between the P5 atoms represented by the low-frequency peak "d" at -127.7 ppm and the other P

atoms contributing to the high frequency peak cluster. To this end, the MAS rotation speed was varied systematically to produce rotational resonance between peak "d" and, successively, the other peaks "a" through "c".

Fig. 7 summarizes the results. The circles are the full widths at half maximum measured for peak "d" when the MAS rotor speed is adjusted to produce rotational resonance with P atoms resonating at the frequency indicated. While the overall width of peak "d" has multiple origins (including chemical shift dispersion, residual ^{31}P-^{7}Li dipole-dipole coupling and ^{31}P-^{31}P scalar coupling) the reintroduction of ^{31}P-^{31}P homonuclear dipole-dipole coupling clearly manifests itself in additional linebroadening effects introduced at rotational resonance. As Fig. 7 illustrates, the effect is significantly stronger with resonances "a" and "c" than with resonance "b". This result confirms the conclusion from the 2-D DQ experiment that there is no direct connectivity between the P-atoms represented by peaks "b"and "d" .

Results from ^{31}P-{^{7}Li} cross-polarization. This experiment is sensitive to the strength of the ^{31}P-^{7}Li dipole-dipole couplings. ^{7}Li single-quantum coherence is spin locked, and magnetization is transferred to the ^{31}P-observe nuclei during a contact time t_c under Hartmann-Hahn matching conditions. Since the rate of magnetization transfer is a function of the heteronuclear dipolar second moment (45), the ^{31}P site differentiation is based on variable contact time CPMAS experiments. Fig. 8 shows typical results. Each spectrum is internally normalized to the most intense resonance "b" so the conclusions are based on relative intensity changes among the peaks within each spectrum. While at long contact times the spectrum resembles the single pulse-MAS NMR result (as expected), resonance "d" is clearly emphasized in the spectrum acquired at the shortest contact time. This result confirms the assignment of resonance "d" to the P5 site. On the other hand it

appears that the difference between ^{7}Li-$^{31}P3$ and ^{7}Li-$^{31}P4$ heteronuclear dipolar coupling strengths (Table 4) is too small to be resolvable by this experiment. Possibly this task might be accomplished by other methods more sensitive to differences in heteronuclear dipolar couplings than variable contact time CPMAS experiments are. Unfortunately, $^{31}P\{^{7}Li\}$ rotational echo double resonance (REDOR) (46) studies carried out with this objective were thwarted owing to the short spin-spin lattice relaxation times associated with these ^{31}P resonances.

Conclusions

Using powerful dipolar solid state NMR techniques, connectivities in the polyphosphide network of LiP_5 have been discerned and characterized. These experiments form a basis for site assignments which are discussed in the context of new, updated crystallographic information. The chemical shift distinctions thus obtained are in good agreement with trends known in the literature: Bonding to an electropositive element such as lithium is associated with strongly negative δ_{iso} values, as also observed in the present study for the resonance of site P5, which carries a formal charge of -1. On the other hand, phosphorus sites whose short range order is dominated by P-P bonding (formal charge of zero) show chemical shifts in the vicinity of zero ppm. In the present study these are the phosphorus sites P1, P2, and P4. For the P3 site, the situation is intermediate: while it also carries a zero formal charge, nevertheless the structure shows that the P3 site is close to the lithium site. This may explain why the P3 resonance is found at more negative chemical shift values than those of the other zerovalent P-atoms. The present study illustrates the power and potential of modern dipolar MAS-NMR experiments for demonstrating connectivities in strongly dipolarly coupled networks. The strategy developed here is currently being applied to other compounds, in order to generate

reliable correlations of ^{31}P chemical shifts with structure and bonding information in solid phosphides.

Acknowledgments

This research was funded by the Deutsche Forschungsgemeinschaft (DFG), by the Wissenschaftsministerium Nordrhein-Westfalen, and by the Fonds der Chemischen Industrie. J.S.a.d.G. thanks the latter institution for a doctoral scholarship. We thank Dipl.-Ing. U. Rodewald for the collection of the four-circle diffractometer data, and K. Wagner for the work at the scanning electron microscope. We are also indebted to the Hoechst AG, Werk Knapsack, and Dr. G. Höfer (Heraeus Quarzschmelze, Hanau) for generous gifts of ultrapure red phosphorus and silica tubes.

References

1. D. E. C. Corbridge, "The Structural Chemistry of Phosphorus", Elsevier, Amsterdam, 1974.
2. H. G. von Schnering and W. Hönle, Enzyclopedia of Inorganic Chemistry, R. B. King, ed., Wiley, London (1994), p. 3105.
3. H. G. von Schnering and W. Hönle, *Chem. Rev.* **88**, 243 (1988).
4. F. Grandjean, A. Gerard, D. J. Braun, W. Jeitschko, *J. Phys. Chem. Solids* **45**, 877 (1984).

5. J. C. Rife, R. N. Dexter, P. M. Bridenbaugh, B. W. Veal, *Phys. Rev. B* **16**, 4491 (1977).

6. C. Sekine, T. Uchiumi, I Shirotani, T. Yagi, *Phys. Rev. Lett.* **79**, 3218 (1997).

7. A. Shaukat, *J. Phys. Chem. Solids* **12**, 1413 (1990).

8. R. Grigorovici, R. Manaila, A. A. Vaipolin, *Acta Crystallogr.* **B24**, 535 (1968).

9. H. Eckert, *Prog. NMR Spectrosc.* **24**, 159 (1992).

10. T. M. Duncan, R. F. Karliczek, W. A: Bonner, F. A. Thiel, *J. Phys. Chem. Solids*, **45**, 389 (1984).

11. M. A: Ryan, M. W: Peterson, D. L. Williamson, J. S. Frey, G. E. Maciel, B. A. Parkinson, *J. Mater. Res.* **2**, 528 (1987).

12. T. A. Vanderah, R. A: Nissan, *J. Phys. Chem. Solids* **49**, 1335 (1988).

13. N. Adolphi, M. S. Conradi, W. E. Buhro, *J. Phys. Chem. Solids* **53**, 1073 (1992).

14. N. L. Adolphi, R. D. Stoddard, S. C. Goel, W. E. Buhro, P. C. Gibbons, M. S. Conradi, *J. Phys. Chem . Solids* **53**, 1275 (1992).

15. S. C. Goel, W. E. Buhro, N. L. Adolphi, M. S. Conradi, *J. Organomet. Chem.* **449**, 9 (1993).

16. K. L. Moran, T. E. Gier, W. T.A. Harrison, G. D. Stucky, H. Eckert, K. Eichele, R. Wasylishen, *J. Am. Chem. Soc.* **115**, 10553 (1993).

17. R. Tycko, G. Dabbagh, S. R. Kurtz, J. P. Goral, *Phys. Rev. B* **45**, 13452 (1992).

18. J. E. McDougall, H. Eckert, G. D. Stucky, N. Herron, and Y. Wang, *J. Am. Chem. Soc.* **111**, 8006 (1989).

19. D. Lathrop, D. Franke, R. Maxwell, T. Tepe, R. Flesher, Z. Zhang, H. Eckert, *Solid State NMR* **1**, 73 (1992).

20. R. A Nissan, T. A. Vanderah, *J. Phys. Chem. Solids* **50**, 347 (1989).

21. D. Mao, P.C. Taylor, Sarah R. Kurtz, M.C. Wu, W.A. Harrison, *Phys. Rev. Lett.* **76**, 4769, (1996).

22. D. Franke, C. Hudalla, H. Eckert, *Solid State NMR* **1**, 297 (1992).

23. D. Franke, K. Banks, H. Eckert, J. *Phys. Chem.* **96**, 11048 (1992).

24. D. Franke, C. Hudalla, R. Maxwell, H. Eckert, *J. Phys. Chem.* **96**, 7506 (1992).

25. D. Franke, C. Hudalla, H. Eckert, *Solid State NMR*, **1**, 33 (1992).

26. H. G. von Schnering and W. Wichelhaus, *Naturwiss.* **59**, 78 (1972).

27. D. Bellavance, J. Mikkelsen, and A. Wold, *J. Solid State Chem.* **2**, 285 (1970).

28. G. P. Felcher, F.A. Smith, D. Bellavance, and A. Wold, *Phys. Rev. B* **3**, 3046 (1971).

29. G. M. Sheldrick, *SHELX-97*, Universität Göttingen (1997).

30. L.M. Gelato and E. Parthé, *J. Appl. Crystallogr.* **20**, 139 (1987).

31. D. J. States, R. A. Haberkorn, D. J. Ruben, *J. Magn. Reson.* **48**, 286 (1982)

32. L. van Wüllen, *Solid State NMR* **13**. 123 (1998).

33. J. H. van Vleck, *Phys. Rev.* **54** ,1168 (1948)

34. D. P. Raleigh, M. H. Levitt, R.G. Griffin, *Chem. Phys. Lett.* **146**, 71 (1988)

35. R. Tycko, G. Dabbagh, *J. Am. Chem. Soc.* **113**, 9444 (1991).

36. N.C. Nielsen, H. Bildsoe, H.J. Jakobsen, M. H. Levitt, *J. Chem. Phys.* **101**, 1805 (1994).

37. D. M. Gregory, D. J. Mitchell, J. A. Stringer, S. Kiihne, J. C. Shiels, J. Callahan, M. A. Mehta, G. P. Drobny, *Chem. Phys. Lett.* **246**, 654 (1995).

38. D. K. Sodickson, M. H. Levitt, S. Vega, R. G. Griffin, *J. Chem. Phys.* **98**, 6742 (1993).

39. Y. K. Lee, N. D. Kurur, M. Helmle, O. G. Johannessen, N. C. Nielsen, M. H. Levitt, *Chem Phys. Lett.* **242**, 304 (1995).

40. M. Baldus, B.H. Meier, *J. Magn. Reson. A,* **121**, 65 (1996).

41. W. A. Dollase, M. Feike, H. Förster, T. Schaller I. Schnell, A. Sebald, S. Steuernagel, *J. Am. Chem. Soc.* **119**, 3807 (1997).

42. M. Feike, R. Graf, I. Schnell, C. Jäger, H. W. Spiess, *J. Am. Chem. Soc.* **118**, 9631 (1996).

43. M. Feike, D. E. Demco, R. Graf, J. Gottwald, S. Hafner, H. W. Spiess, *J. Magn. Reson. A*, **122**, 214 (1996).

44. H. Geen, J. Gottwald, R. Graf, I. Schnell, H. W. Spiess, J.J. Titman, *J. Magn. Reson.* **125**, 224 (1997).

45. M. Mehring, Principles of High Resolution NMR in Solids, Springer, Berlin, Heidelberg, New York, 1983.

46. T. Gullion, J. S. Schaefer, *J. Magn. Reson.* **41**, 196 (1989).

Figure Captions

Figure 1: A cut-out of the polyanionic phosphorus network of LiP_5. The thermal ellipsoids are drawn at the 90% probability limit. Single-digit numbers correspond to the atom designations.

Figure 2: Stereographic drawing of the crystal structure of LiP_5. Lithium atoms are represented by black spheres.

Figure 3: Atomic coordinations in LiP_5. The environments of the lithium atoms (black ellipsoids) as resulting from the structure refinements in the centrosymmetric group *Pnam* (the suggested high temperature modification) and from the refinement in the acentric group $Pna2_1$ are shown in the upper part of the figure. The phosphorus environments correspond to the refinement in the space group $Pna2_1$. The thermal ellipsoids are drawn at the 90% probability limit. The lithium atoms of the refinement in *Pnam* occupy split positions on both sides of the mirror plane. Single-digit numbers correspond to the atom designations; the interatomic distances are indicated in pm units.

Figure 4: 202.5 MHz single-pulse ^{31}P MAS-NMR spectra of LiP_5 at different rotation frequencies: top: 8 kHz, bottom: 16 kHz. Peaks "a" through "d" and their corresponding spinning sidebands (asterisks) are indicated.

Figure 5: Pulse sequence used for 2-D exchange spectroscopy with double quantum filtering. The bottom part illustrates the coherence pathway selected by phase cycling.

Figure 6: DQ-filtered ^{31}P- two-dimensional exchange spectrum of crystalline LiP_5. Connectivities are indicated by off-diagonal peaks.

Figure 7: Rotational Resonance spectroscopy of LiP_5: The linewidth of the -127.7 ppm peak assigned to the P5 site is plotted as a function of the rotational frequency difference between this peak and the point in the spectrum indicated by filled squares.

Figure 8: Variable contact time $\{^7Li\}^{31}P$ CPMAS spectra of LiP_5. The contact times used are indicated. A single-pulse ^{31}P MAS spectrum is shown for comparison. Each spectrum has been internally normalized to the most intense resonance "b"

TABLE 1

Crystal Data for LiP_5[a]

Space group	*Pnam* (No. 62)	*Pna*2_1 (No. 33)
Formula units/cell	$Z = 4$	
Formula mass	161.81	
a (pm)	1043.7(1)	
b (pm)	658.92(8)	
c (pm)	654.90(9)	
V (nm^3)	0.45038(9)	
Calculated density (g/cm^3)	2.386	
Crystal size (μm^3)	$25 \times 50 \times 350$	
$\theta/2\theta$ up to	$2\theta = 100°$	
Range in h, k, l	$\pm 22, \pm 14, -14 \leq l \leq 2$	
Highest/lowest transmission	1.10	
Total number of reflections	11639	
Inner residual (I)	$R_i = 0.0307$	$R_i = 0.0301$
Unique reflections	2469	2965
Reflections with $I_0 > 2\sigma(I_0)$	1961	2357
Number of variables	38	56
Conventional residual (F)	$R = 0.067$	$R = 0.020$
Weighted residual (F^2)	$R_w = 0.145$	$R_w = 0.054$

[a] The correct symmetry for LiP_5 at room temperature is *Pna*2_1 (space group No.33). However, the structure can also be refined with split lithium positions and half occupancy in the centrosymmetric group *Pnam*, a non-standard setting of the space group *Pnma*.

TABLE 2

Atomic Parameters of LiP_5[a]

Atom	*Pnam*	*x*	*y*		*z*	B_{eq}
Li	8*d*	0.080(2)	0.045(3)		0.632(3)	3.1(3)
P1	8*d*	0.08923(7)	0.5929(1)		0.4925(1)	0.809(9)
P3	4*c*	0.1938(1)	0.4222(2)		¼	0.75(1)
P4	4*c*	0.19099(9)	0.4436(1)		¾	0.68(1)
P5	4*c*	0.1287(1)	0.1093(2)		¼	1.29(2)
Atom	$Pna2_1$	*x*	*y*	*z*	$z' = z + ¼$	B_{eq}
Li	4*a*	0.0780(3)	0.0452(6)	0.3881(7)	0.6381(7)	3.30(7)
P1	4*a*	0.41428(3)	0.08698(4)	0.25729(4)	0.50729(4)	0.716(4)
P2	4*a*	0.09233(3)	0.59825(4)	0.24282(4)	0.49282(4)	0.718(4)
P3	4*a*	0.19363(2)	0.42261(3)	0[b]	¼[b]	0.689(3)
P4	4*a*	0.19116(2)	0.44326(3)	0.49964(8)	0.74964(8)	0.719(3)
P5	4*a*	0.12858(2)	0.10915(3)	0.01523(8)	0.26523(8)	1.115(5)
Atom	B_{11}	B_{22}	B_{33}	B_{12}	B_{13}	B_{23}
Li	2.01(10)	4.40(15)	3.50(17)	0.06(10)	0.74(11)	1.64(15)
P1	0.769(7)	0.803(8)	0.575(9)	–0.017(6)	0.030(8)	0.051(10)
P2	0.808(7)	0.774(9)	0.572(9)	0.004(5)	0.024(9)	–0.011(10)
P3	0.701(6)	0.810(6)	0.557(6)	0.042(4)	0.013(10)	–0.022(12)
P4	0.754(6)	0.818(6)	0.583(6)	–0.090(5)	0.013(10)	0.018(11)
P5	0.644(6)	0.824(6)	1.878(13)	0.034(5)	–0.085(10)	–0.002(10)

[a] The phosphorus positions can be refined in the centrosymmetric space group *Pnam*, where the lithium atoms occupy a split position with half occupancy. The parameters of this refinement are listed in the upper part of the table. The true symmetry of LiP_5 at room temperature is that of the polar space group $Pna2_1$. The results of this refinement are listed in the lower parts of the table. The atom labels of the two refinements correspond to each other. The P1 atoms of the position 8*d* of *Pnam* correspond to the P1 and P2 atoms of the refinement in $Pna2_1$. The positional parameters of the refinement in $Pna2_1$ were standardized with the program STRUCTURE TIDY (30). For better comparison of the refinements in the two space groups the positional parameter $z' = z + ¼$ is listed in the middle part of the table. The thermal parameters *B* are expressed in units of $nm^2 \times 100$.

[b] These z parameters were not allowed to vary in order to define the origin of this polar space group.

TABLE 3

Interatomic Distances and P–P–P Angles in the Structure of LiP_5[a]

Li:	P5	252.5(3)	P2: P4	222.2(1)	P4: P5	217.8(1)
	P5	253.4(5)	P1	222.5(1)	P2	222.2(1)
	P3	262.1(3)	P3	223.3(1)	P1	222.6(1)
	P4	296.8(4)	Li	309.9(4)	Li	296.8(4)
	P1	308.7(4)	P3: P5	217.6(1)	P5: P3	217.6(1)
	P2	309.9(4)	P1	222.9(1)	P4	217.8(1)
P1:	P2	222.5(1)	P2	223.3(1)	Li	252.5(3)
	P4	222.6(1)	Li	262.1(3)	Li	253.4(5)
	P3	222.9(1)				
	Li	308.7(4)				

P2–P1–P4	98.47(2)	P5–P3–P1	109.64(1)
P2–P1–P3	100.71(2)	P5–P3–P2	108.16(1)
P4–P1–P3	94.82(2)	P1–P3–P2	90.96(1)
P4–P2–P1	95.93(1)	P5–P4–P2	101.87(1)
P4–P2–P3	94.65(2)	P5–P4–P1	100.26(1)
P1–P2–P3	98.13(1)	P2–P4–P1	98.56(3)
		P3–P5–P4	101.81(1)

[a] All distances shorter than 355 pm (Li–P) and 315 pm (P–P), respectively, are listed.

TABLE 4

^{31}P MAS NMR Peak Assignments and Selective Dipolar ^{31}P - ^{31}P and ^{31}P - ^{7}Li Second Moments [10^6 s^{-2}] Calculated From the Structure of Crystalline LiP_5

	P1	P2	P3	P4	P5
P1(-11.5ppm)	6.3	71.5	67.3	67.2	16.7
P2(-11.5ppm)	71.5	5.8	67.9	66.5	16.5
P3(-29.0ppm)	67.2	66.5	4.4	21.7	72.3
P4(+1.8 ppm)	67.3	67.9	21.7	4.5	72.7
P5(-128 ppm)	16.8	16.5	72.3	72.7	4.6
Li1	34.8	34.2	58.7	38.7	118.3

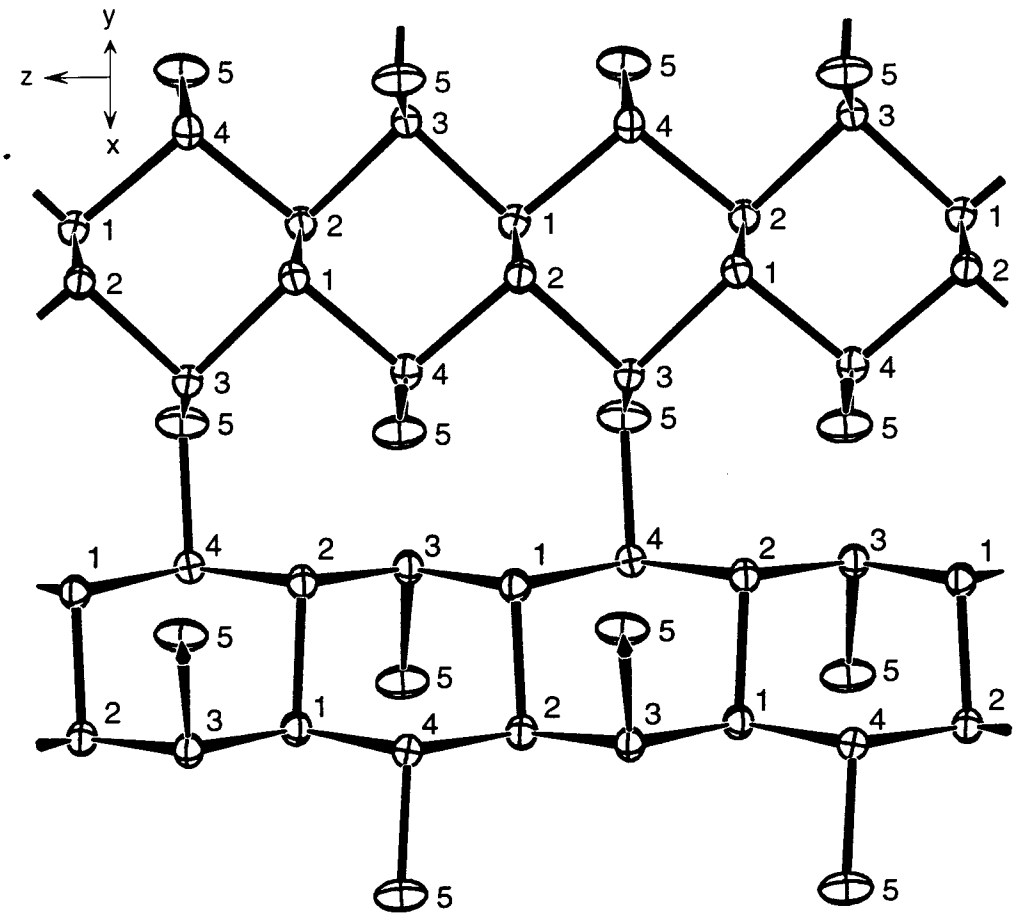

FIG. 1. A cut-out of the polyanionic phosphorus network of LiP_5. The thermal ellipsoids are drawn at the 90% probability limit. Single-digit numbers correspond to the atom designations.

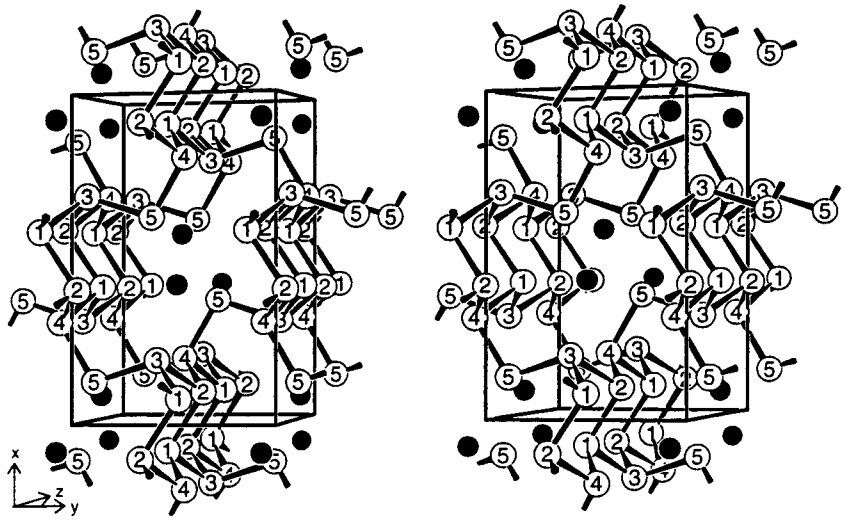

FIG. 2. Stereographic drawing of the crystal structure of LiP_5. Lithium atoms are represented by black spheres.

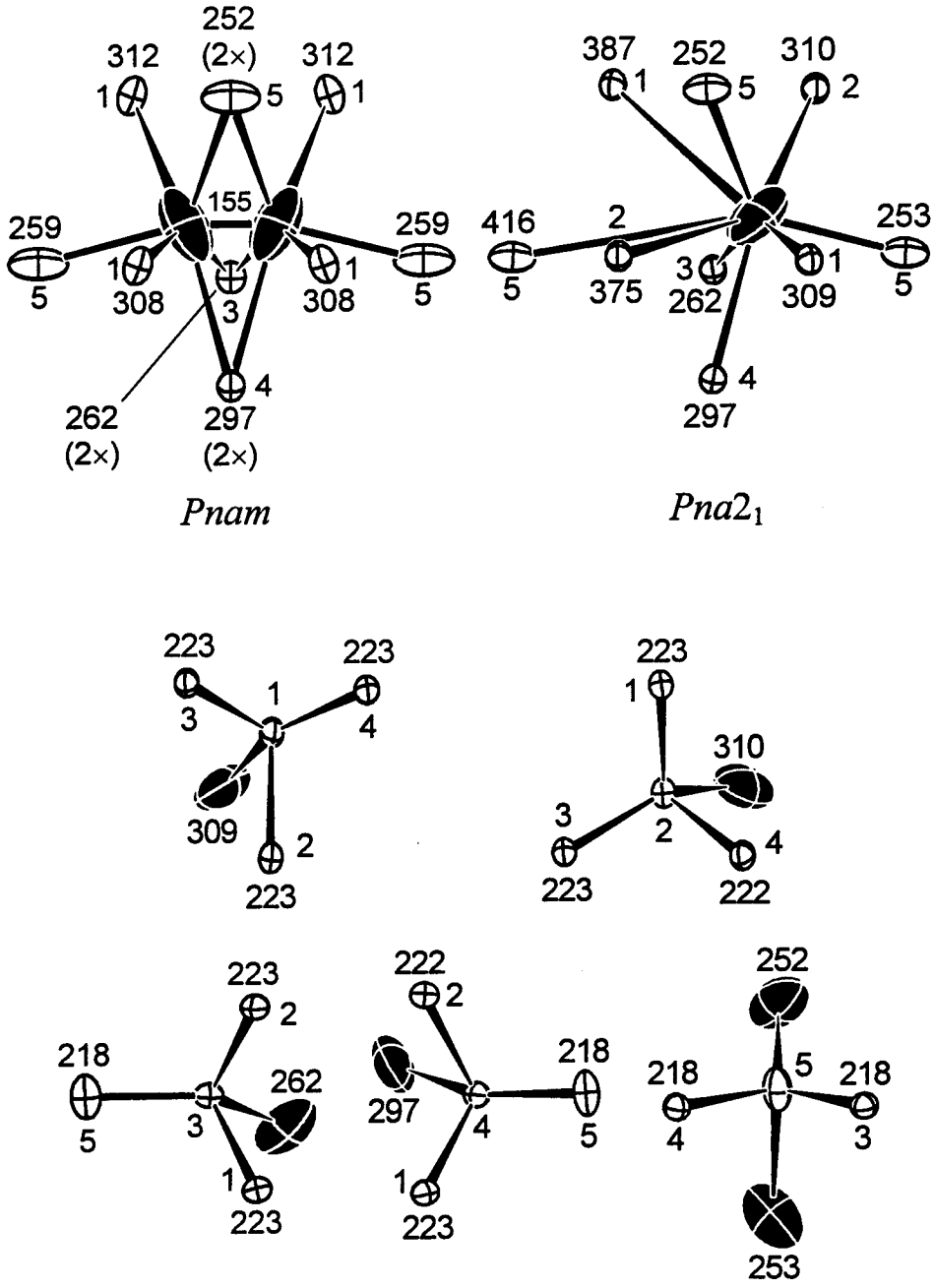

FIG. 3. Atomic coordinations in LiP_5. The environments of the lithium atoms (black ellipsoids) as resulting from the structure refinement in the centrosymmetric group *Pnam* (the suggested high temperature modification) and from the refinement in the acentric group $Pna2_1$ are shown in the upper part of the figure. The phosphorus environments correspond to the refinement in the space group $Pna2_1$. The thermal ellipsoids are drawn at the 90% probability limit. The lithium atoms of the refinement in *Pnam* occupy split positions on both sides of the mirror plane. Single-digit numbers correspond to the atom designations; the interatomic distances are indicated in pm units.

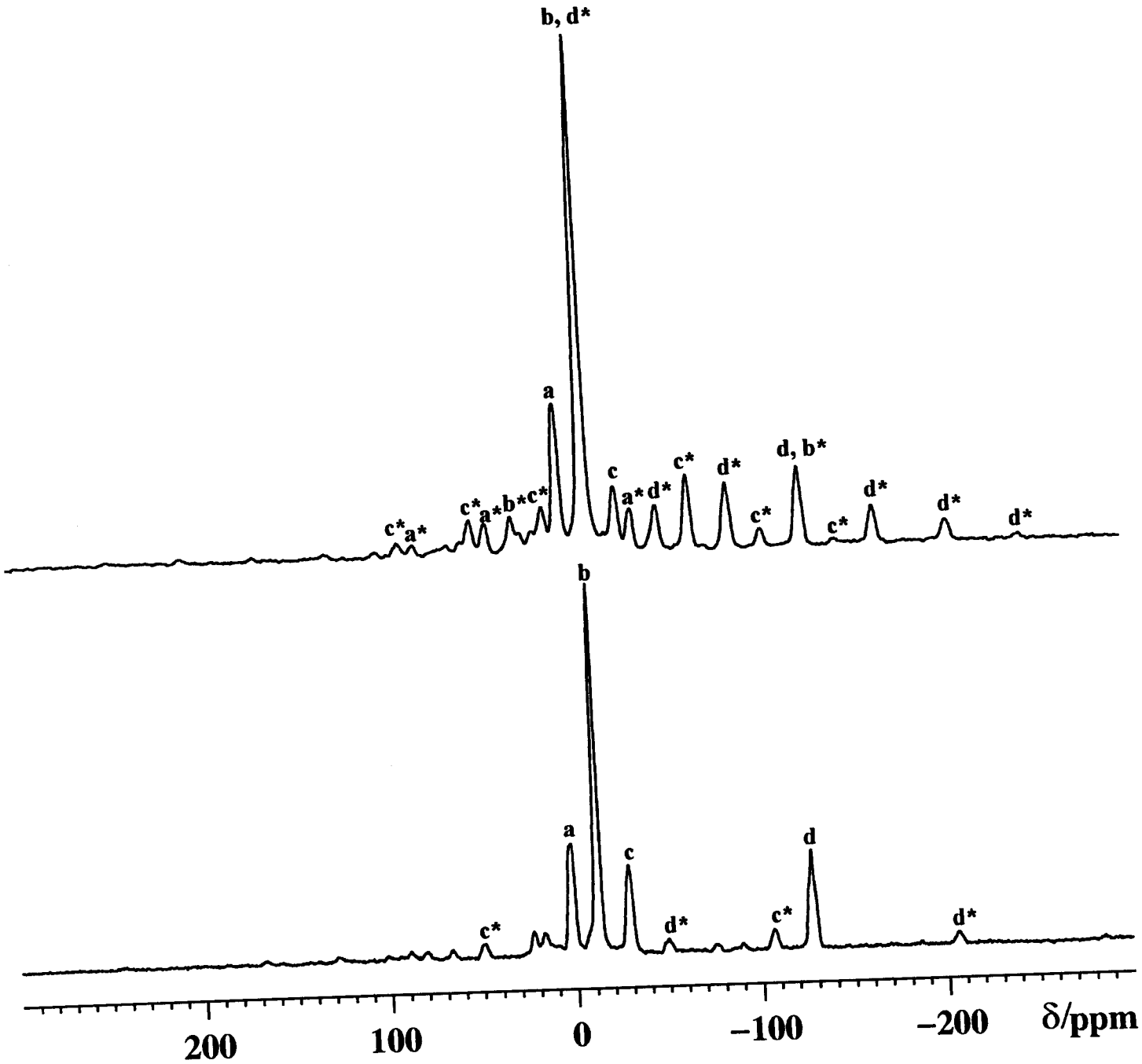
b, d*
a
c
a*
d*
c*
d*
d, b*
c*
d*
c*
d*
c*
a*
b*
c*
c*
a*
d*
c*
b
a
c
d
c*
d*
c*
d*
200
100
0
–100
–200
δ/ppm

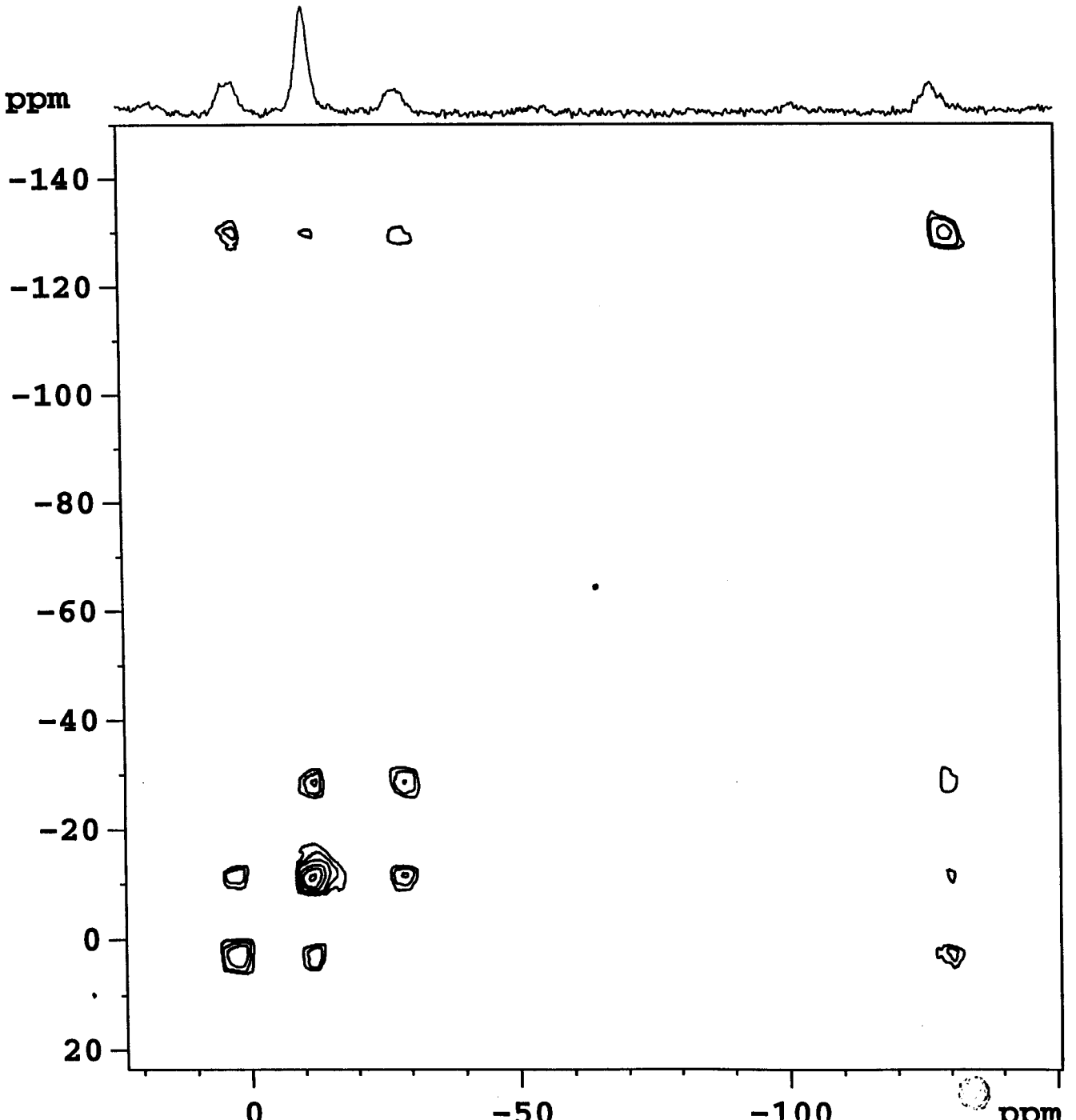
ppm
-140
-120
-100
-80
-60
-40
-20
0
20
0
-50
-100
ppm

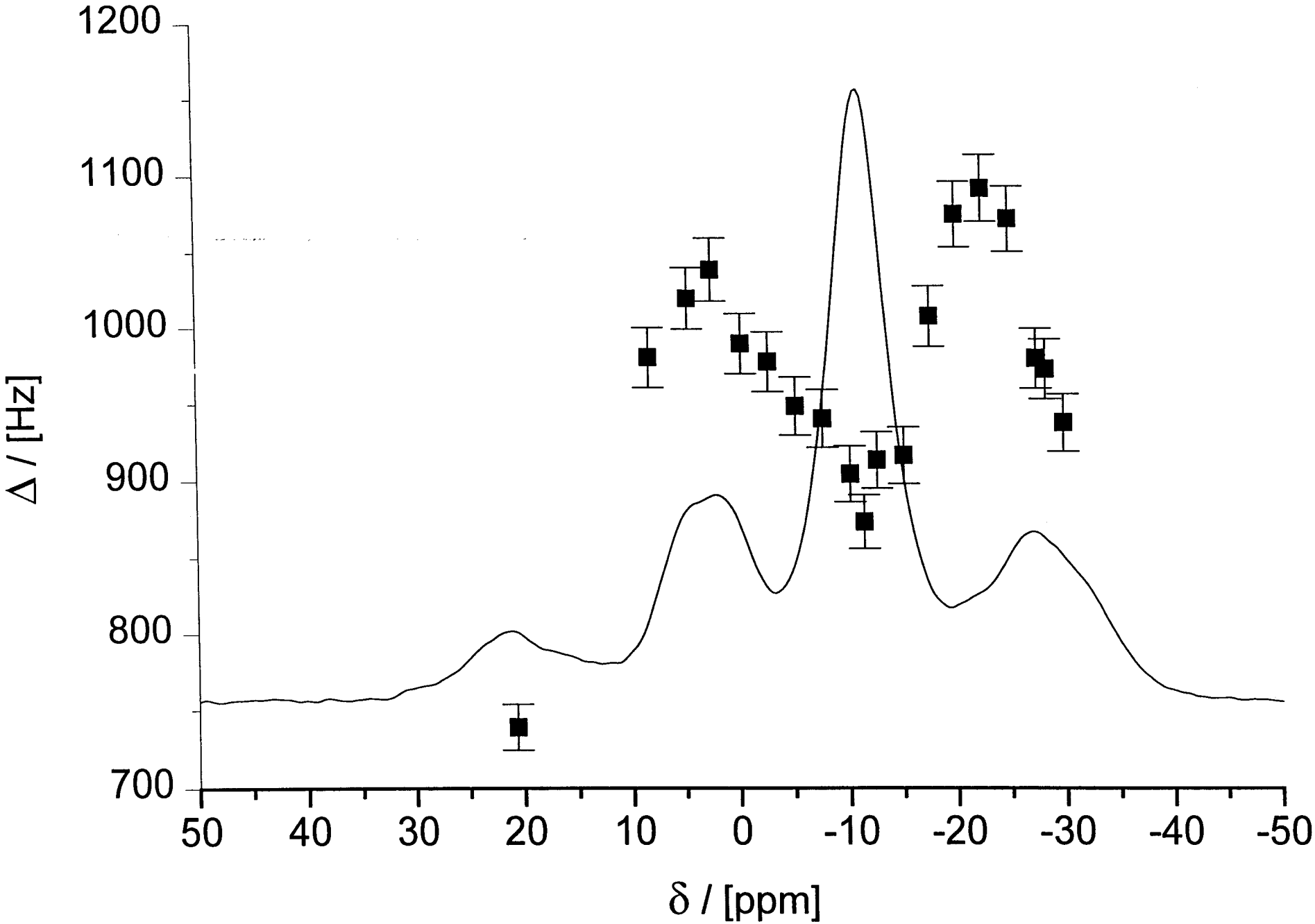
1200
1100
1000
900
800
700
Δ / [Hz]
50
40
30
20
10
0
-10
-20
-30
-40
-50
δ / [ppm]

^{7}Li-^{31}P CPMAS LiP_5: